

Examining the Gap in the Chirp Mass Distribution of Binary Black Holes

VAIBHAV TIWARI¹ AND ALBERTO VECCHIO¹

¹*Institute of Gravitational Wave Astronomy,
School of Physics and Astronomy, University of Birmingham,
Edgbaston, Birmingham B15 2TT, UK*

ABSTRACT

The mass distribution of binary black holes inferred from gravitational wave measurements is expected to shed light on their formation scenarios. An emerging structure in the mass distribution indicates the presence of multiple peaks around chirp masses of $8M_{\odot}$, $14M_{\odot}$, and $27M_{\odot}$. In particular, there is a lack of observations between chirp masses of 10 and $12M_{\odot}$. In this letter, we report that observations significantly favour the model supporting suppression of the rate in a narrow chirp mass range compared to the model that doesn't include suppression at a confidence greater than 99.5%. Using another test, which measures the deviation between the inferred chirp mass distributions from the two models, we conservatively estimate a 95% confidence in the presence of a feature. A lack of confidence has been reported in the presence of a gap around a comparable location in the component mass distribution. The differing conclusions are due to a unique correlation between the primary (heavier of the two masses) and the secondary (lighter of the two masses) masses of binary black holes. This correlation results in increased clustering of measured chirp masses around specific values.

Keywords: Gravitational wave astronomy(675); Gravitational wave sources(677); Compact binary stars(283)

1. INTRODUCTION

The chirp mass of a compact binary with masses m_1 and m_2 is given by

$$\mathcal{M} = \frac{(m_1 m_2)^{3/5}}{(m_1 + m_2)^{1/5}}. \quad (1)$$

Chirp mass dominates the phase evolution of gravitational wave (GW) and, therefore, is the most accurately measured parameter (Cutler & Flanagan 1994). However, it is not a parameter of astrophysical importance. It is not expected that channels responsible for forming and merging compact binaries will leave an imprint on the chirp mass distribution. These imprints, which may appear as peaks or gaps, can be visible in the chirp mass due to their presence in mass parameters of astrophysical importance, such as the primary or component mass.

The total number of Binary Black Hole (BBH) after the culmination of LIGO-Virgo-KAGRA (LVK) collaborations third observation run (O3) is 69 (Aasi et al. 2015; Acernese et al. 2015; Akutsu et al. 2021). These observations have been observed with a false alarm rate of at least one per year. Figure 1 shows these observations' chirp mass/redshift measurements. The chirp mass measurements cluster around specific mass values, resulting in peaks and gaps in the inferred chirp mass distribution (Tiwari & Fairhurst 2021; Li et al. 2021; LVK 2023; Tiwari 2022, 2024a). Investigations have also aimed at peaks observed in the primary mass distribution (e.g. see Edelman et al. (2023); Toubiana et al. (2023); Farah et al. (2023)).

Figure 1 shows a lack of observations in the range $10\text{--}12M_{\odot}$. This range, which we may refer to as *gap*, but could also be a narrow local minima, has been explained as a feature of isolated binary evolution of stripped stars (Schneider et al. 2021, 2023) or failed supernova mechanism (Disberg & Nelemans 2023). The unique location of peaks has also been suggested as arising due to a hierarchical merger scenario when the first peak is formed by the merger of Black Hole (BH) of stellar origin and successive peaks by the repeated merger of remnants (Tiwari & Fairhurst

2021; Tiwari 2022). Follow-up analyses have fit the prominent peaks in the primary mass distribution using similar proposals (Mahapatra et al. 2025). Such a proposal potentially explains the depleted rate between the two peaks¹.

Considering these unconventional proposals, confidence in the presence of this feature must be well understood. Presence of a gap in the component mass range $10\text{--}15M_{\odot}$ was investigated by Adamcewicz et al. (2024). They reported non-observation of a gap in this mass range. Galaudage & Lamberts (2025) investigated the presence of *polluting* observations that would fill the gap in the component mass distribution. However, a sharp drop and rise of the inferred chirp mass distribution suggest the presence of a feature and raise the question of how it could leave a gap in the chirp mass distribution, which requires an explanation.

In this article, we focus on the chirp mass range $9.5\text{--}20M_{\odot}$, at either end of which is the presence of a prominent peak. We estimate the confidence in the presence of gap in this chirp mass range. This article is laid out as follows. In Section 2 we describe the method. In Section 3, we discuss our investigations, and in Section 5, we discuss our findings.

2. METHOD

Vamana is a Gaussian mixture model framework to infer the BBH population (Tiwari 2021). The components of the mixture models are three-dimensional multivariate normals that model the chirp mass, mass ratio and aligned spins (component aligned with the orbital angular momentum). Each component also includes a power law to measure the evolution of the merger rate with the redshift. It is a Bayesian analysis; thus, the inference is made by drawing many possible distributions calculated from hyperparameter posteriors. We employ three flavours of Vamana to perform our investigation. The first flavour is a mixture model with no constraints on the location of the Gaussian modelling the chirp mass. The second flavour restricts the location of Gaussians and exclusively uses a power-law to infer the distribution in the range $9.5\text{--}20M_{\odot}$. The second flavour has been set up to avoid inferring a local maximum or minimum in this range. The third flavour is identical to the second flavour but with extra hyperparameters to suppress density in narrow chirp mass regions. These flavours are labelled as \mathbb{M} , \mathbb{M}_{pl} , and \mathbb{M}_{pl+gap} respectively and are described in Appendix B.

We first investigate the presence of a gap by analysing if \mathbb{M}_{pl} has a better or poorer fit with the GW observations compared to the two remaining models. The standard approach when comparing two models is to calculate the Bayes factor, which indicates the preferred model.

$$\mathcal{B} = \frac{p(\mathbf{d}|\mathbb{M}_1)}{p(\mathbf{d}|\mathbb{M}_2)} = \frac{\int p_1(\Lambda) [\int \mathcal{L}(\mathbf{d}|\theta) p_1(\theta|\Lambda) d\theta] d\Lambda}{\int p_2(\Lambda) [\int \mathcal{L}(\mathbf{d}|\theta) p_2(\theta|\Lambda) d\theta] d\Lambda}, \quad (2)$$

where θ are the modeled parameters, and \mathbf{d} is the data. Λ and $p(\Lambda)$ are the model hyperparameters and their priors respectively. \mathcal{L} is the likelihood of observing data \mathbf{d} if gravitational waves were emitted by a binary with parameters θ . $p(\theta|\Lambda)$ is the functional form of the model. The term inside the square brackets is the conditional marginal likelihood, which is used in sampling the hyperparameter posterior.

The Bayes factor is sensitive to the choice of the hyperparameter prior. For example, for the model \mathbb{M}_{pl+gap} , the prior on the extra hyperparameters controlling the gap can be adjusted to increase or decrease Bayes factor in comparison to model \mathbb{M}_{pl} ; thereby incorrectly concluding presence or absence of a gap. We overcome this situation by integrating the numerator and denominator in Equation 2 only for hyperparameters which meaningfully contribute to the posterior. We achieve this by first sampling a fixed number of hyperparameter posteriors for a model and choosing the smallest conditional marginal likelihood as the threshold above which integrals in Equation 2 are calculated next. As most of the priors are uniform, in effect, we are calculating the Bayes factors corresponding to the most optimal priors for the models. However, the estimated quantity is not a Bayes factor in the usual sense.

We use an additional statistic to assess the presence of a gap: a weighted sum of squared deviations between the chirp mass distributions inferred from model \mathbb{M}_{pl} and the other two models. We quantify the departure between two distributions by defining a quantity

$$\chi^2 = \sum_i \frac{(\mu_1(\mathcal{M}_i) - \mu_2(\mathcal{M}_i))^2}{\sigma_1(\mathcal{M}_i) \sigma_2(\mathcal{M}_i)} \quad (3)$$

¹ However, depending on rate, intergenerational mergers will fill this gap.

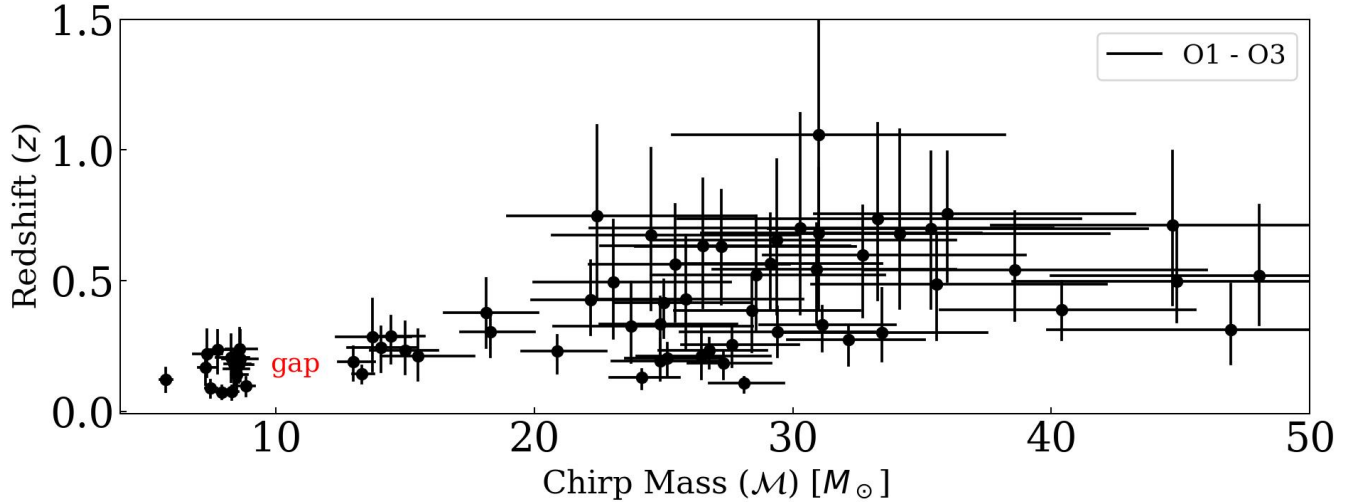


Figure 1. The measured chirp mass and redshift value of the 69 BBH observed with a false alarm rate of once per year or less. Observations cluster around a chirp mass value of $8M_{\odot}$ and $14M_{\odot}$, leaving a gap in between.

where μ_1 and μ_2 are the mean density, and σ_1 and σ_2 are the standard deviation of the inferred chirp mass from models 1 and 2. The population from the two models is inferred on discrete mass values, \mathcal{M}_i . The summation in Equation 3 is done for values between $9.5M_{\odot}$ and $20M_{\odot}$. The bins are placed at an interval of $0.1M_{\odot}$. The magnitude of χ^2 depends on the difference between the mean distributions inferred from the two models and the accuracy with which these means were estimated.

For both the statistics, we set the second models to be always \mathbb{M}_{pl} , which does not infer a feature, and make comparisons with the distribution inferred from model \mathbb{M}_{pl+gap} or \mathbb{M} capable of inferring local maxima or minima. To convert the statistics to p-values, we use a fiducial chirp mass distribution for simulating multiple catalogs after mimicking the observations and measurement process. We choose the mean inferred distribution from model \mathbb{M}_{pl} as the fiducial distribution. This choice is data-informed and ensures that the simulated catalogs have a comparable number of observations to the real catalog in the chirp mass range of $9.5\text{--}20 M_{\odot}$. Similarly, we choose data-informed distributions of mass ratio and aligned spin. Using our models, we infer populations from each of the simulated catalog. By following this procedure, we accumulate BF/χ^2 values corresponding to astrophysical chirp mass distribution that is assumed to be featureless and describes the data best. Finally, the $\text{BF}_{\text{obs}}/\chi_{\text{obs}}^2$ of the GW observations are compared against values from the simulated catalogs. We have described the creation of simulated catalogs in Appendix A.

3. INVESTIGATION

We investigate whether the observations can be confidently explained as just another draw from the fiducial distribution, i.e. in reality, the underlying distribution is featureless and the observed chirp mass values are just one among many possible draws from it. In this section, we perform two comparisons. First, we investigate a gap characterised by sharp decay in density in a narrow chirp mass range using models \mathbb{M}_{pl} and \mathbb{M}_{pl+gap} . In our second investigation, we relax the shape of the gap and draw our conclusion by comparing models \mathbb{M}_{pl} and \mathbb{M}

3.1. Comparing \mathbb{M}_{pl} and \mathbb{M}_{gap+pl}

Figure 2 shows the inferred chirp mass distribution using models \mathbb{M}_{pl} and \mathbb{M}_{pl+gap} . As expected, the distribution inferred from model \mathbb{M}_{pl} does not show the presence of a local minimum or maximum in the chirp mass range $9.5\text{--}12M_{\odot}$. However, the distribution inferred from model \mathbb{M}_{pl+gap} shows a modulation. We calculate the Bayes factor and χ^2 values for the GW observations by using Equations 2 and 3. To quantify confidence in this feature, we also calculate these values for the simulated catalogs. They are shown in Figure 3 for the 500 catalogs we simulate. We find that none of the simulated catalog has a Bayes factor value larger than the one calculated for the observations. This suggests at least 99.5% confidence in the presence of a gap. However, 10% of the simulated catalogs have χ^2 values larger than the one estimated for the observations, suggesting a smaller 90% confidence in the presence of a gap. This is a conservative test, as we observe in the simulated catalogs that a large χ^2 often arises due to an overall

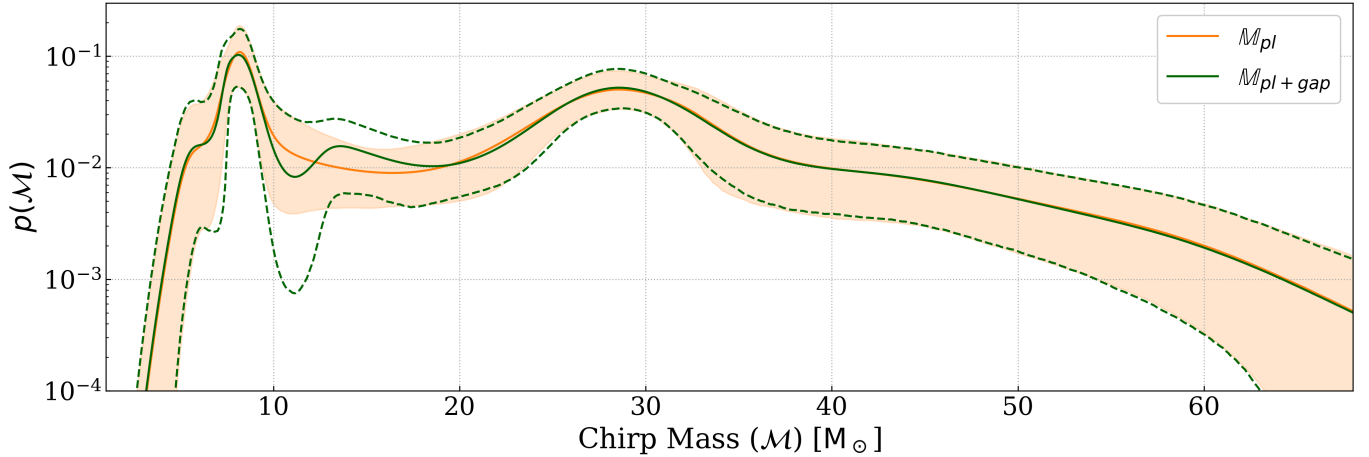


Figure 2. The chirp mass distribution inferred from the models \mathbb{M}_{pl} and \mathbb{M}_{pl+gap} . The solid line represents the mean distribution, and the shaded region or dashed line indicates the 90% credible interval. As expected, the orange curve does not exhibit features in the chirp mass range of $9.5\text{--}20 M_{\odot}$. It is used as the fiducial chirp mass distribution for creating simulated catalogs. The models infer almost identical distributions except in the range $9.5\text{--}20 M_{\odot}$.

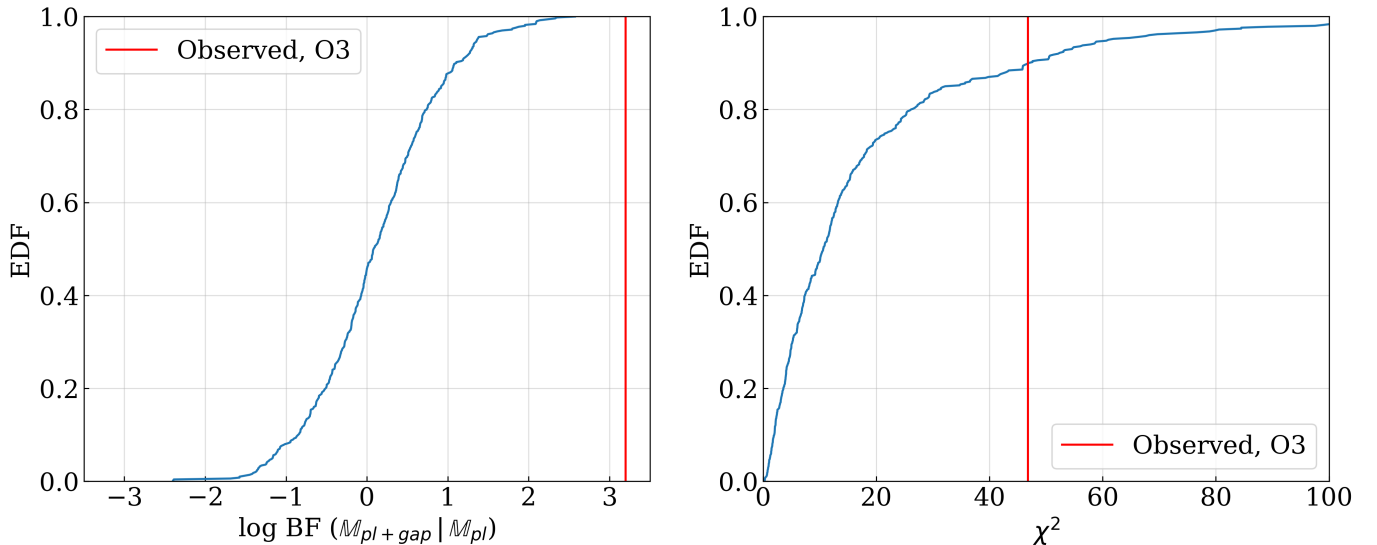


Figure 3. The log Bayes factor (left) and χ^2 values (right) between models \mathbb{M}_{pl+gap} and \mathbb{M}_{pl} for the 500 simulated catalog. The red lines indicate the estimated values for the GW observations.

difference between the distributions inferred from the two models and not because of the presence of a local minimum in the distribution inferred by the model \mathbb{M}_{pl+gap} .

3.2. Comparing \mathbb{M}_{pl} and \mathbb{M}

Next, we repeat this procedure for \mathbb{M}_{pl} and \mathbb{M} . Figure 4 shows the inferred chirp mass distribution using these models. Model \mathbb{M} is more flexible in inferring a variety of distributions compared to the model \mathbb{M}_{pl+gap} . Its mean distribution shows a larger modulation than \mathbb{M}_{pl+gap} ; however, the credible intervals are also larger. Figure 5 shows the Bayes factor and χ^2 values between the two models for the simulated catalogs. We find that none of the simulated catalog has a Bayes factor value larger than the one calculated for the observations. This suggests at least 99.5% confidence in the presence of a gap. However, 5% catalogs have χ^2 larger than the value for the GW observation, suggesting a 95% confidence in the presence of a gap. This is a conservative test, as χ^2 can be large with or without the presence of a gap-like feature; i.e., a large χ^2 only implies that two models have inferred distributions that differ.

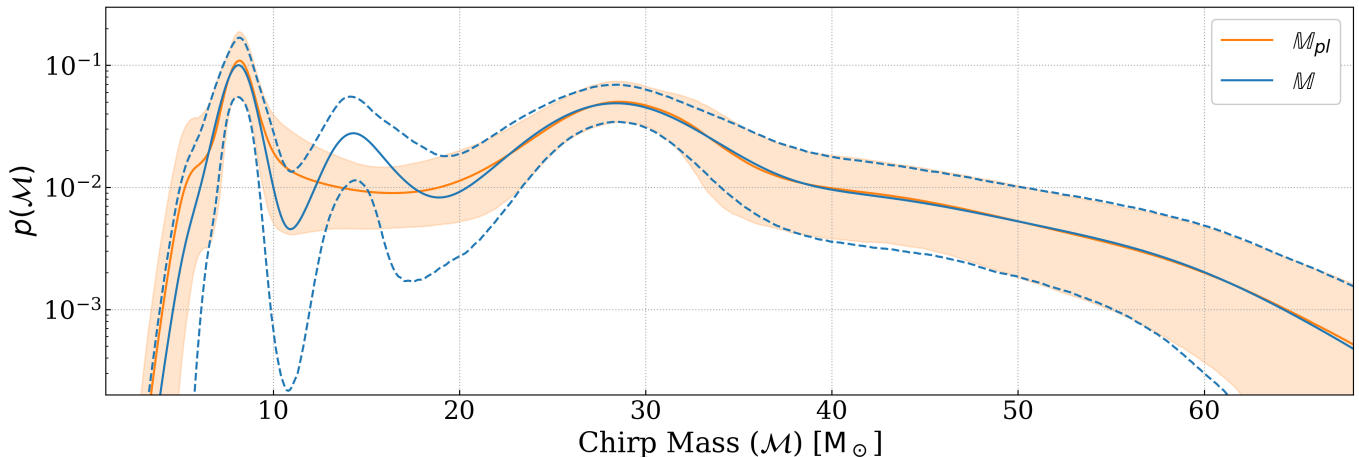


Figure 4. The chirp mass distribution inferred from the models \mathcal{M}_{pl} and \mathcal{M}_{pl+gap} . The solid line represents the mean distribution, and the shaded region or dashed line indicates the 90% credible interval. The models infer a similar distribution except in the range $9.5\text{--}20M_{\odot}$.

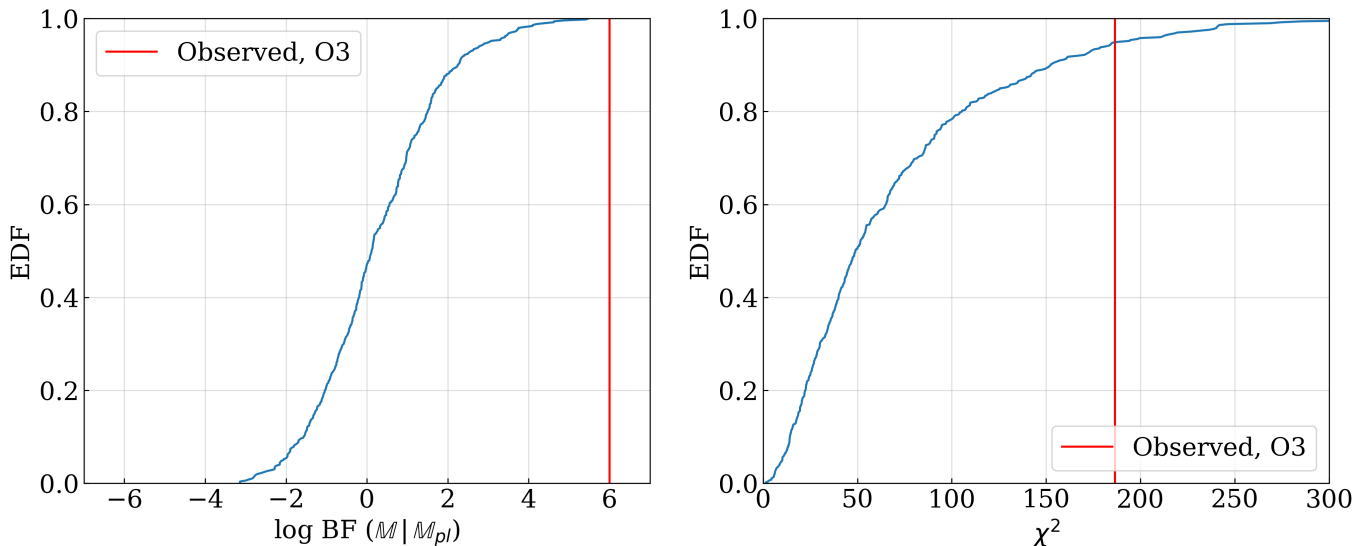


Figure 5. The log Bayes factor (left) and χ^2 values (right) between models \mathcal{M}_{pl+gap} and \mathcal{M}_{pl} for the 500 simulated catalog. The red lines indicate the estimated values for the GW observations.

Unlike the previous section, which estimates the confidence in the presence of a gap characterised by suppression of density in a narrow chirp mass range, in this analysis, we are calculating the confidence in the feature inferred by the model \mathcal{M} . The mean distribution in Figure 4 suggests this feature may be a gap, or a gap followed by a peak.

4. A UNIQUE CORRELATION

Based on our tests, we can conclude that observations in GWTC-3 suggest the presence of a gap in the chirp mass range $9.5\text{--}12 M_{\odot}$. In their analysis [Adamcewicz et al. \(2024\)](#) conclude against the presence of a gap in the component mass range $10\text{--}15M_{\odot}$. They raise an important point about the pairing function: a gap in the chirp mass distribution, when combined with a mass-ratio distribution that follows a power-law with a spectral index of $\beta = 2$, results in a much shallower gap in the primary or secondary mass distribution (Please see their Appendix A). Therefore, the presence of a gap in the chirp mass distribution does not necessarily imply a gap in the component mass distribution. Chirp mass is the most accurately measured parameter and is expected to be the least biased. But chirp mass is not a parameter of astrophysical importance. For a gap to exist in chirp mass, the primary and secondary masses

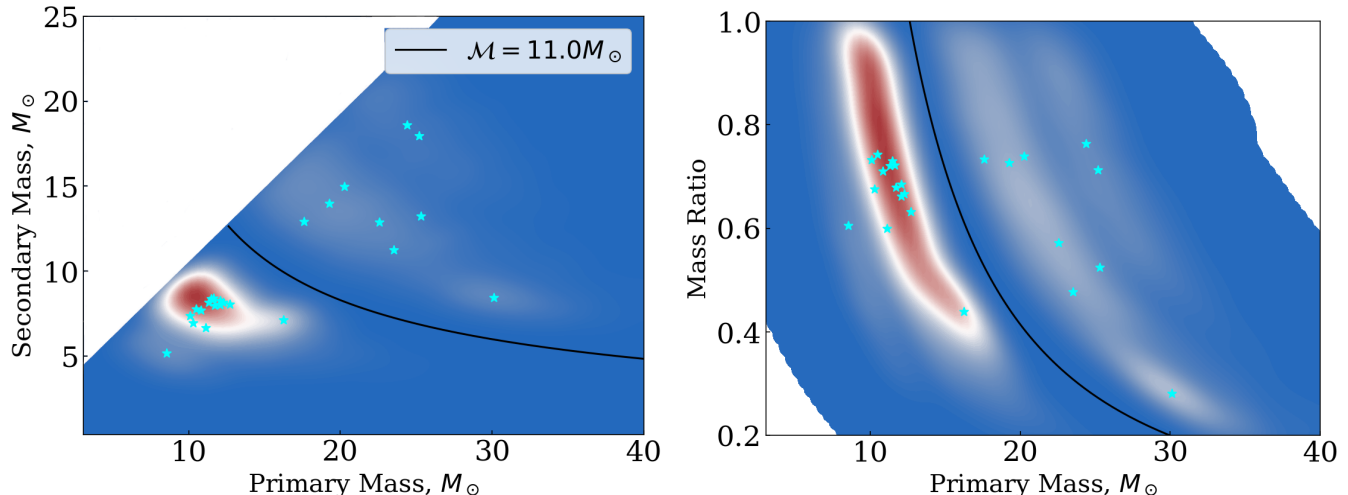


Figure 6. The mass estimates of BBHs measured from the GWs stacked a 2D density plot. Only binaries measured with mean chirp mass larger than $5M_{\odot}$ and smaller than $20M_{\odot}$ have been included. The stars are the median values measured for the individual BBHs. The black curve shows a constant $=11.0M_{\odot}$ line.

should combine uniquely. A larger primary mass should pair with a smaller secondary mass, and vice versa. Figure 6 shows all the mass measurements made from the GWs stacked in a 2D density plot. The plot only includes binaries measured with a mean chirp mass greater than $5M_{\odot}$ and smaller than $20M_{\odot}$. This plot qualitatively shows a unique combination of the two masses that results in increased clustering of chirp masses around specific values compared to other mass parameters. Naturally, the existence of these correlations affects the implications we draw from the mass distribution inferred from GWs. We estimated confidence in the presence of the $14M_{\odot}$ in [Tiwari \(2024a\)](#). A discussion similar to this sub-section is also present there.

5. DISCUSSION

In this letter, we investigate the observed gap in the chirp mass distribution. We estimate the presence of a gap with a confidence level greater than 99.5% based on model comparison using Bayes factors. However, when comparing models using a much more conservative χ^2 statistic, we infer the presence of a gap with a confidence level greater than 95%. Independent analyses have reported the absence of a gap in a comparable mass range for the component mass distribution. We qualitatively demonstrate that this is due to a unique correlation between the primary and secondary mass values, resulting in increased clustering of chirp mass values around specific values compared to other mass parameters. The number of GW are expected to quadruple in the next few months. This roughly implies a factor of two reduction in the size of confidence bands for the inferred distributions. There will be a sufficient number of observations to make robust estimation of the confidence in the primary features of the binary black hole mass distribution. A persistent feature in the chirp mass distribution, which is absent in other mass parameters, certainly raises questions. Chirp mass is the most accurately measured parameter and least affected by any biases; however, it is not a parameter of astrophysical importance. Therefore, presence of a strong feature in the chirp mass distribution requires a careful explanation.

¹ Thanks to Sukant Bose for LIGO’s Publications & Presentations review and to Tom Dent for the helpful feedback. This work was conducted on Cardiff University’s HAWK HPC, supported by STFC grants ST/I006285/1 and ST/V005618/1.

² This material is based upon work supported by NSF’s LIGO Laboratory which is a major facility fully funded by the National Science Foundation.

A. SIMULATING GRAVITATIONAL WAVE CATALOG

In this analysis, the network comprises advanced LIGO Livingston and Hanford detectors (Aasi et al. 2015). We draw uniformly on right ascension, declination, coalescence phase, polarisation angle, cosine of the inclination angle and square of the luminosity distance. The coalescence time is fixed to zero. Simulated injections are generated using IMRPHENOMD (Husa et al. 2016; Khan et al. 2016). This model is optimised for binary systems with spins aligned with the orbital angular momentum. It contains only the leading (2,2) harmonic; therefore, precession and higher harmonics have not been accounted for. Thus, we draw chirp mass, mass ratio and two aligned spin components. Any signal that crosses a signal-to-noise ratio (SNR) of 9.0 is tagged as *observed* and selected for parameter estimation. We do not keep track of parameter draws but ensure that the *observed* signals follow the distribution listed in Table 1. The parameters are estimated using the non-Markovian parameter sampler Varaha (Tiwari et al. 2023; Tiwari 2024b). The parameter sampler uses a uniform prior on the chirp mass, mass ratio, aligned spin components and the square of luminosity distance.

The network SNR threshold used to tag simulated signals as *observed* has been chosen carefully. Parameters for a lower SNR signal are estimated with a larger error than those with a higher SNR. A threshold of 9.0 has been chosen to ensure comparable measurement errors between simulated injections and GW measurements. Moreover, parameter estimation uses the standard Bayesian analysis; thus, parameters retain the same correlation as observed in real signals. We performed 2,500 parameter estimation runs with masses and spins distribution listed in Table 1. We maintain the mass ratio and spin distribution intact for the investigations presented in this article, while drawing from the fiducial chirp mass distributions through importance sampling.

B. MODELS USED IN POPULATION INFERENCE

Vamana infers population using a mixture of components. The inferred distributions are truncated between 0.05 and 1.0 for mass ratio and -0.9 and 0.9 for aligned spins. We assume aligned spins to be identically but independently distributed. We utilise 10 components for all inferences and employ identical settings when inferring astrophysical and simulated populations. The models used in our investigations are presented in Table 2:

i) Model $\mathbb{M}_{\mathcal{M}}$: This model infers the joint distribution of chirp mass, mass ratio and aligned spin distributions. Components are multivariate normals in this model. The cross-terms for the covariance matrix between different parameters are set to zero, except for the covariance between the chirp mass and the mass ratio. This allows the mixture model to infer variation of mass ratio with chirp mass flexibly. Thus, model $\mathbb{M}_{\mathcal{M}}$ essentially consists of components composed of a bivariate normal and a univariate normal distributions. This is described in Equation B1.

$$p(\mathcal{M}, q, \chi_1, \chi_2 | \Lambda) = \sum_{i=1}^N w_i \mathcal{N}(\mathcal{M}, q | \mu_i^{\mathcal{M}}, \sigma_i^{\mathcal{M}}, \mu_i^q, \sigma_i^q, C_i^{\mathcal{M}q}) \phi(\chi_1 | \mu_i^{\chi}, \sigma_i^{\chi}) \phi(\chi_2 | \mu_i^{\chi}, \sigma_i^{\chi}), \quad (\text{B1})$$

where N is the number of components, w are the weights for the components in the mixture, $C^{\mathcal{M}q}$ is the covariance between the chirp mass parameter and mass ratio, μ and σ are the location and scale of the Gaussians.

ii) Model \mathbb{M}_{pl} : This model restricts the location of Gaussians to enforce an inference that is featureless between

Table 1. Distribution of the *observed* (corresponding to signals that from cross a network SNR of 9.0) mass and spin parameters of the simulated population.

	Parameter	Distribution
Chirp Mass	\mathcal{M}	$p(\mathcal{M}) \propto \mathcal{M}^{-1/2}, \quad \mathcal{M} \in [4.0, 65.0]$
Mass Ratio	q	$p(q) \propto q^{-5/2}, \quad q \in [0.2, 1]$
Aligned spin of the heavier object	s_{1z}	$p(s_{1z}) = \mathcal{N}(\mu = 0, \sigma = 0.15)$
Aligned spin of the lighter object	s_{2z}	$p(s_{2z}) = \mathcal{N}(\mu = 0, \sigma = 0.15)$

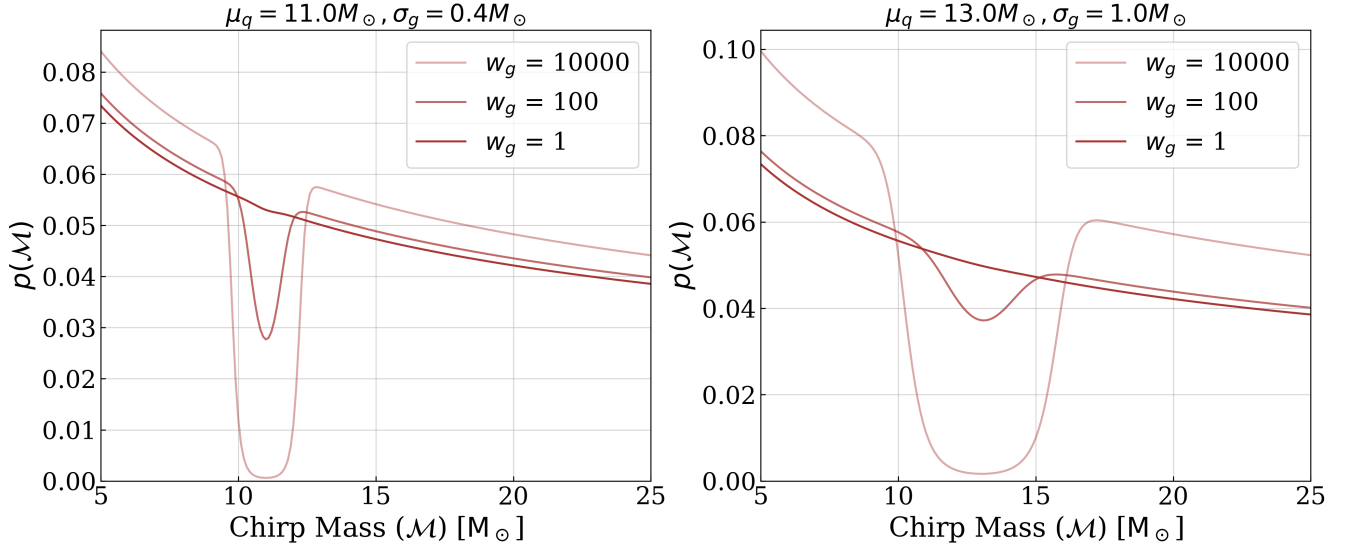


Figure 7. This figure plots the function defined in the Equation B3 for several values of hyperparameter. The power law truncates at $5.0M_{\odot}$ and $25M_{\odot}$ and has a spectral index of -0.4 .

the two prominent peaks observed in the mass distribution. The intermediate-mass range is inferred using one component composed of a power-law to infer the chirp mass distribution and two univariate normals to infer the aligned spin and mass ratio distributions.

$$p(\mathcal{M}, q, \chi_1, \chi_2 | \Lambda) = \prod_{i=1}^N w_i f(\mathcal{M}, q) \phi(\chi_1 | \mu_i^{\chi}, \sigma_i^{\chi}) \phi(\chi_2 | \mu_i^{\chi}, \sigma_i^{\chi}),$$

$$f(\mathcal{M}, q) = \begin{cases} \mathcal{N}(\mathcal{M}, q | \mu_i^m, \sigma_i^m, \mu_i^q, \sigma_i^q, C_i^{\mathcal{M}q}), & i = 1 \cdots N-1 \\ \mathcal{P}(\mathcal{M} | \alpha^{\mathcal{M}}, \mathcal{M}_{\min}, \mathcal{M}_{\max}) \phi(q | \mu_N^q, \sigma_N^q), & i = N \end{cases} \quad (\text{B2})$$

The model \mathbb{M}_{pl+gap} is identical to \mathbb{M}_{pl} but includes extra hyperparameters to suppress density in the narrow chirp mass range. The suppressed density is defined as,

$$p(\mathcal{M}) = \frac{p_{pl}(\mathcal{M})}{1 + w_g \phi(\mu_g, \sigma_g)/100}, \quad (\text{B3})$$

where $p_{pl}(\mathcal{M})$ is the power-law distribution and ϕ is the normal distribution with mean μ_g and scale σ_g . These hyperparameters control the location and width of the gap. Hyperparameter w_g controls the depth of the gap. We use priors, $\mu_g \sim \mathcal{U}(9M_{\odot}, 20M_{\odot})$, $\sigma_g \sim \mathcal{U}(0.2M_{\odot}, 1.0M_{\odot})$, and $w_g \sim \text{Log-}\mathcal{U}(1, 10000)$. Figure 7 plots the distribution in Equation B3 for several values of hyperparameters.

The BBH population is inferred using the observations with a false alarm rate of at most once per year. We only used observations reported by the LVK collaborations (LIGO Scientific Collaboration & Virgo Collaboration 2019; Abbott et al. 2021, 2024, 2023). Only observations with a mean chirp mass greater than $5M_{\odot}$ are used. We excluded GW190814 and any observation consistent with a binary neutron star and neutron star-black hole binary from our investigations. The total number of observations chosen is 69. In addition, to reduce computational cost, we did not correct for selection effects and fixed the redshift evolution to be uniform in comoving coordinates. We don't expect this correction to introduce a feature in the target mass range and impact our conclusions. The binary parameters are estimated in the detector frame; we assume the Planck15 cosmology (Ade et al. 2016) to change to the source frame quantities.

Table 2. This table lists the hyperparameters of the three models used to infer the BBH population. The last column identifies the model where the hyperparameters are used. U stands for Uniform, and UL for Uniform-in-log.

Λ	Description/Modeled Parameter	Prior	Range	Models
w_i	Mixing weights, w	Dirichlet(α), $\alpha_{1\dots N} = 1/N$	0–1	\mathbb{M} , \mathbb{M}_{pl}
μ_i^q	Gaussian’s location, q	UL	.05–1.04	\mathbb{M} , \mathbb{M}_{pl}
σ_i^q	Gaussian’s scale, q	U	$0.1 - 1.0 / \sqrt{N}$	\mathbb{M} , \mathbb{M}_{pl}
μ_i^X	Gaussian’s location, s_z	U/UL	$ \chi_i < 0.4 / 0.4 < \chi_i < 0.9$	\mathbb{M} , \mathbb{M}_{pl}
σ_i^X	Gaussian’s scale, s_z	U	$0.1 - 1.3 / \sqrt{N}$	\mathbb{M} , \mathbb{M}_{pl}
$\mu_i^{\mathcal{M}}$	Gaussian’s location, \mathcal{M}	U	$5M_{\odot} - 60M_{\odot}$	\mathbb{M}
$\mu_i^{\mathcal{M}}$	Gaussian’s location, \mathcal{M}	U	$5M_{\odot} - 9M_{\odot}$, $25M_{\odot} - 60M_{\odot}$	\mathbb{M}_{pl}
$\sigma_i^{\mathcal{M}}$	Gaussian’s scale, \mathcal{M}	U	$0.05 \mu_i^{\mathcal{M}} / \sqrt{N} - 0.185 \mu_i^{\mathcal{M}} / \sqrt{N}$	\mathbb{M} , \mathbb{M}_{pl}
$C_i^{\mathcal{M}q}$	Covariance, $\mathcal{M}-q$	U	$-0.5 \sigma_i^{\mathcal{M}} \sigma_i^q - 0.5 \sigma_i^{\mathcal{M}} \sigma_i^q$	\mathbb{M} , \mathbb{M}_{pl}
\mathcal{M}_{\min}	Powerlaw lower edge, \mathcal{M}	U	$6M_{\odot} - 9.5M_{\odot}$	\mathbb{M}_{pl}
\mathcal{M}_{\max}	Powerlaw higher edge, \mathcal{M}	U	$28.5M_{\odot} - 80M_{\odot}$	\mathbb{M}_{pl}
$\alpha^{\mathcal{M}}$	Powerlaw slope, \mathcal{M}	U	-3–3	\mathbb{M}_{pl}

REFERENCES

- Aasi, J., Abbott, B. P., Abbott, R., Abbott, T., et al. 2015, *Classical and Quantum Gravity*, 32, 074001, doi: [10.1088/0264-9381/32/7/074001](https://doi.org/10.1088/0264-9381/32/7/074001)
- Abbott, R., Abbott, T. D., Abraham, S., et al. 2021, *Physical Review X*, 11, 021053, doi: [10.1103/PhysRevX.11.021053](https://doi.org/10.1103/PhysRevX.11.021053)
- Abbott, R., Abbott, T. D., Acernese, F., et al. 2023, *Physical Review X*, 13, 041039, doi: [10.1103/PhysRevX.13.041039](https://doi.org/10.1103/PhysRevX.13.041039)
- . 2024, *PhRvD*, 109, 022001, doi: [10.1103/PhysRevD.109.022001](https://doi.org/10.1103/PhysRevD.109.022001)
- Acernese, F., et al. 2015, *Classical and Quantum Gravity*, 32, 024001, doi: [10.1088/0264-9381/32/2/024001](https://doi.org/10.1088/0264-9381/32/2/024001)
- Adamcewicz, C., Lasky, P. D., Thrane, E., & Mandel, I. 2024, *ApJ*, 975, 253, doi: [10.3847/1538-4357/ad7ea8](https://doi.org/10.3847/1538-4357/ad7ea8)
- Ade, P. A. R., Aghanim, N., Arnaud, M., et al. 2016, *A&A*, 594, A13, doi: [10.1051/0004-6361/201525830](https://doi.org/10.1051/0004-6361/201525830)
- Akutsu, T., et al. 2021, *Progress of Theoretical and Experimental Physics*, 2021, 05A101, doi: [10.1093/ptep/ptaa125](https://doi.org/10.1093/ptep/ptaa125)
- Cutler, C., & Flanagan, E. E. 1994, *Phys. Rev. D*, 49, 2658, doi: [10.1103/PhysRevD.49.2658](https://doi.org/10.1103/PhysRevD.49.2658)
- Disberg, P., & Nelemans, G. 2023, *A&A*, 676, A31, doi: [10.1051/0004-6361/202245693](https://doi.org/10.1051/0004-6361/202245693)
- Edelman, B., Farr, B., & Doctor, Z. 2023, *ApJ*, 946, 16, doi: [10.3847/1538-4357/acb5ed](https://doi.org/10.3847/1538-4357/acb5ed)
- Farah, A. M., Edelman, B., Zevin, M., et al. 2023, *ApJ*, 955, 107, doi: [10.3847/1538-4357/aced02](https://doi.org/10.3847/1538-4357/aced02)
- Galadage, S., & Lamberts, A. 2025, *A&A*, 694, A186, doi: [10.1051/0004-6361/202451654](https://doi.org/10.1051/0004-6361/202451654)
- Husa, S., Khan, S., Hannam, M., et al. 2016, *PhRvD*, 93, 044006, doi: [10.1103/PhysRevD.93.044006](https://doi.org/10.1103/PhysRevD.93.044006)
- Khan, S., et al. 2016, *Phys. Rev. D*, 93. <https://journals.aps.org/prd/abstract/10.1103/PhysRevD.93.044007>
- Li, Y.-J., Wang, Y.-Z., Han, M.-Z., et al. 2021, *ApJ*, 917, 33, doi: [10.3847/1538-4357/ac0971](https://doi.org/10.3847/1538-4357/ac0971)
- LIGO Scientific Collaboration, & Virgo Collaboration. 2019, *Physical Review X*, 9, 031040, doi: [10.1103/PhysRevX.9.031040](https://doi.org/10.1103/PhysRevX.9.031040)
- LVK. 2023, *Physical Review X*, 13, 011048, doi: [10.1103/PhysRevX.13.011048](https://doi.org/10.1103/PhysRevX.13.011048)
- Mahapatra, P., Chattopadhyay, D., Gupta, A., et al. 2025, *PhRvD*, 111, 023013, doi: [10.1103/PhysRevD.111.023013](https://doi.org/10.1103/PhysRevD.111.023013)
- Schneider, F. R. N., Podsiadlowski, P., & Laplace, E. 2023, *ApJL*, 950, L9, doi: [10.3847/2041-8213/acd77a](https://doi.org/10.3847/2041-8213/acd77a)
- Schneider, F. R. N., Podsiadlowski, P., & Müller, B. 2021, *A&A*, 645, A5, doi: [10.1051/0004-6361/202039219](https://doi.org/10.1051/0004-6361/202039219)
- Tiwari, V. 2021, *Classical and Quantum Gravity*, 38, 155007, doi: [10.1088/1361-6382/ac0b54](https://doi.org/10.1088/1361-6382/ac0b54)
- . 2022, *ApJ*, 928, 155, doi: [10.3847/1538-4357/ac589a](https://doi.org/10.3847/1538-4357/ac589a)
- . 2024a, *MNRAS*, 527, 298, doi: [10.1093/mnras/stad3155](https://doi.org/10.1093/mnras/stad3155)
- . 2024b, *arXiv e-prints*, arXiv:2405.16568, doi: [10.48550/arXiv.2405.16568](https://doi.org/10.48550/arXiv.2405.16568)
- Tiwari, V., & Fairhurst, S. 2021, *ApJL*, 913, L19, doi: [10.3847/2041-8213/abfb7](https://doi.org/10.3847/2041-8213/abfb7)

Tiwari, V., Hoy, C., Fairhurst, S., & MacLeod, D. 2023,
PhRvD, 108, 023001, doi: [10.1103/PhysRevD.108.023001](https://doi.org/10.1103/PhysRevD.108.023001)

Toubiana, A., Katz, M. L., & Gair, J. R. 2023, MNRAS,
524, 5844, doi: [10.1093/mnras/stad2215](https://doi.org/10.1093/mnras/stad2215)